Photoacoustics 43 (2025) 100708

Contents lists available at ScienceDirect

Photoacoustics

journal homepage: www.elsevier.com/locate/pacs

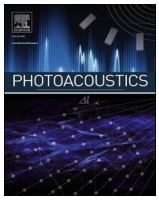

Optical synchronous signal demodulation-based quartz-enhanced photoacoustic spectroscopy for remote, multi-point methane detection in complex environments

Bo Sun [a,d], Tingting Wei [e], Mingjiang Zhang [a,d], Lijun Qiao [a,d], Zhe Ma [a,d], Angelo Sampaolo [b,c], Pietro Patimisco [b,c], Vincenzo Spagnolo [b,c,*], Hongpeng Wu [b,c,*], Lei Dong [b,c,*]

[a] College of Physics and Optoelectronics, Taiyuan University of Technology, Taiyuan 030024, China
[b] State Key Laboratory of Quantum Optics and Quantum Optics Devices, Institute of Laser Spectroscopy, Shanxi University, Taiyuan 030006, China
[c] PolySense Lab—Dipartimento Interateneo di Fisica, University and Politecnico of Bari, Bari, Italy
[d] Shanxi Key Laboratory of Precision Measurement Physics, Taiyuan University of Technology, Taiyuan 030024, China
[e] State Key Laboratory for Modern Optical Instrumentation, Center for Optical & Electromagnetic Research, College of Optical Science and Engineering, International Research Center for Advanced Photonics, Zhejiang University, Zijingang Campus, Hangzhou 310058, China

ARTICLE INFO

Keywords:
Optical synchronized signal demodulation (OSSD)
Quartz-enhanced photoacoustic spectroscopy (QEPAS)
Remote gas sensing
Methane detection
Sewer monitoring

ABSTRACT

We present a novel optical synchronized signal demodulation (OSSD) method applied in quartz-enhanced photoacoustic spectroscopy (QEPAS) for remote gas sensing. Using 1 % of the laser source as an optical synchronization signal, kilometer-scale remote gas detection was achieved, overcoming the challenges of long-distance real-time detection in complex environments with conventional QEPAS. A time-sharing OSSD-QEPAS system for sewer methane detection was subsequently developed. The system's modulation depth was optimized, and the catalytic effect of water vapor on photoacoustic signals was validated, resulting in a CH_4 sensor achieving a detection limit of 445 ppb with a 300-ms averaging time, and an excellent linear dynamic range with a $R^2 = 0.999$. To demonstrate the stability, robustness, and accuracy of the OSSD-QEPAS system, continuous methane measurements covering a 14-hour period at two different sewer locations on campus were performed.

1. Introduction

Optical-based trace gas detection has been extensively studied and widely applied in demanding fields requiring remote monitoring, such as industrial emissions control, environmental pollution assessment, and safety inspections of specialized equipment [1–6]. These applications demand high-precision measurements, where effective signal demodulation plays a pivotal role. The performance of laser-based gas sensors is inherently tied to the accuracy of the laser's synchronous signal. However, high-cost lasers deployed in challenging environments are vulnerable to safety risks posed by dust, temperature fluctuations, humidity, and other external factors, necessitating reliable remote synchronous signal transmission [7,8].

Traditional gas sensors typically rely on electrical signal transmission for demodulation. However, transmitting electrical signals over long distances using materials like copper or aluminum incurs significant costs and is highly susceptible to electromagnetic interference. Furthermore, long-distance electrical transmission often leads to signal distortion and reduced signal-to-noise ratios due to resistance in metallic conductors. Common solutions, such as using amplifiers or thicker wires, only partially mitigate these issues and impose additional constraints, restricting the laser position near the measurement site. These limitations hinder the practicality of remote signal demodulation and restrict the broader adoption of optical detection systems in remote sensing applications.

To address the challenges of significant signal loss, high noise, elevated costs, and other limitations associated with long-distance electrical signal transmission, this study proposes a novel optical signal synchronous demodulation (OSSD) method. In OSSD, synchronous signals are transmitted through optical fibers, replacing traditional electrical wiring. A photodetector (PD) converts the optical synchronous signals carried by the laser beam into electrical signals, which are

* Corresponding authors at: State Key Laboratory of Quantum Optics and Quantum Optics Devices, Institute of Laser Spectroscopy, Shanxi University, Taiyuan 030006, China.
E-mail addresses: vincenzoluigi.spagnolo@poliba.it (V. Spagnolo), wuhp@sxu.edu.cn (H. Wu), donglei@sxu.edu.cn (L. Dong).

https://doi.org/10.1016/j.pacs.2025.100708
Received 4 February 2025; Received in revised form 24 February 2025; Accepted 26 February 2025
Available online 27 February 2025

subsequently processed by the demodulation module to determine target gas concentrations. By leveraging the nearly lossless transmission properties of optical fibers, this method enables reliable remote synchronous signal transmission, significantly expanding the effective gas detection range. For long-distance signal transmission, optical fibers provide several key advantages. First of all, a superior transmission performance. Indeed, optical signal attenuation in fibers is more than an order of magnitude lower per kilometer compared to electrical signals transmitted through the highest-capacity coaxial cables available. For instance, at commonly used optical communication wavelengths (e.g., 1550 nanometers), the attenuation of single-mode optical fibers is typically less than 0.2 dB/km, whereas high-capacity coaxial cables can experience attenuation levels of 10 dB/km or more [9–11]. This significant reduction in attenuation ensures the preservation of signal strength over long distances, making optical fibers a superior choice for applications demanding high signal integrity and extended transmission ranges. Additionally, optical fiber offers several practical advantages, including its compact size, lightweight nature, high corrosion resistance, and excellent immunity to electromagnetic interference. These characteristics make fiber-based systems easier to install and maintain while ensuring long-term stability, even in harsh environments. The abundance and low cost of fiber materials contribute to the overall cost-effectiveness of the system [12,13].

By leveraging OSSD for trace gas detection, the laser source can be safely positioned several kilometers away from the detection point, which is particularly beneficial for operations in complex environments such as power plants, mines, and dense forests. Furthermore, incorporating transfer switches at the laser ports enables time-sharing monitoring of gas concentrations across multiple locations. This approach significantly reduces operational costs while enhancing efficiency, making OSSD a highly practical and scalable solution for remote gas sensing applications.

Over the past decade, trace gas sensors utilizing photoacoustic spectroscopy (PAS) technology based on laser absorption spectroscopy [14], have been extensively adopted across various gas detection applications due to their high sensitivity, exceptional selectivity, and minimal background noise [15–18]. PAS operates by detecting acoustic signals generated during the deexcitation process that occurs when gas molecules interact with a modulated laser. At the core of PAS sensors lies the photoacoustic cell, which typically operates within a resonant frequency range of 1–10 kHz, enabling efficient detection of the generated acoustic signals.

However, PAS technology still has certain limitations, including high costs, large system volume, and susceptibility to environmental noise. In recent years, quartz-enhanced photoacoustic spectroscopy (QEPAS), a specialized variant of PAS, has been extensively studied and applied across various fields [19–26]. QEPAS retains the key advantages of PAS while significantly reducing both the size and cost of the acoustic detection module (ADM) and enhancing resistance to environmental noise, making it a more efficient and practical solution for gas sensing applications. In QEPAS, a quartz tuning fork (QTF) coupled with two metallic tubes, acting as acoustic resonators, serves as the spectrophone. The QTFs are characterized by a resonance frequency of tens of kHz, enhancing the acoustic detection module's (ADM) ability to mitigate environmental noise and ensuring more stable and reliable measurements. With its cost-effectiveness, compact design, and superior noise immunity, QEPAS is particularly well-suited for validating the feasibility of OSSD. These advantages make it an ideal platform for advancing OSSD technology and driving further research in the field. What's more, the sensor performance can be improved when the custom QTFs are used [24,27–29].

Methane (CH_4) is a primary component of natural gas, oil, and coal mine gas. It is a colorless, odorless, and highly combustible greenhouse gas with significant implications for global warming, with human activities responsible for approximately 70 % of atmospheric CH_4 emissions. In sewers, CH_4 is primarily generated by the decomposition of organic matter and is a major contributor to atmospheric CH_4 levels. Under poorly ventilated conditions, sewer CH_4 concentrations can exceed 5 %, reaching the lower explosive limit (LEL) of CH_4, which ranges from 5 % to 15 %. At such levels, CH_4 poses severe explosion risks as well as environmental and safety hazards [30]. Given these concerns, real-time CH_4 monitoring in sewers is critical, necessitating the development of innovative and cost-effective detection technologies. While various sewer CH_4 sensors have been proposed [31–37], the use of an affordable distributed feedback (DFB) laser in combination with QEPAS for this application remains unexplored. This study focuses on addressing this gap by leveraging QEPAS technology for enhanced CH_4 detection in sewer environments.

We demonstrated here OSSD as a novel and effective solution to overcome the limitations of existing QEPAS gas sensors, particularly the challenges associated with long-distance remote signal transmission. By utilizing a lossless optical synchronous signal, OSSD addresses key issues such as high costs, limited detection range, laser susceptibility to environmental damage, and safety concerns inherent in traditional electrical signal demodulation. In this approach, the optical signal detected by the photodetector (PD) is compared with the modulated signal applied to the laser, ensuring accurate and reliable remote demodulation. To demonstrate its practicality, a QEPAS-based CH_4 sensor integrated with OSSD was developed and deployed for continuous, real-time CH_4 monitoring over a 14-hour period at two distinct sewer wells. The results confirm the feasibility of OSSD for long-range, cost-effective, and safe trace gas detection in complex environments.

2. Optical synchronous signal demodulation principle

Laser demodulation technology utilizes a laser beam as a carrier for transmitting low-frequency signals. In this case, the laser operates at a much higher carrier frequency, enabling more precise and efficient signal transmission, particularly over long distances. Laser modulation typically falls into two main categories: wavelength modulation and intensity modulation. OSSD employs wavelength modulation, where the laser's wavelength is varied by modulating the input current. When a sinusoidal modulated current signal $a(t) = A\cos w_m t$ is applied to the laser, the corresponding output wavelength can be expressed as:

$$\lambda(t) = \lambda_0 + \Delta\lambda\cos w_m t\# \quad (1)$$

A and w_m represent the modulation depth and angular frequency of the modulated current, defined as $w_m = 2\pi f_m$, while λ_0 is the laser central emission wavelength and $\Delta\lambda$ is the wavelength change amplitude during modulation. Since the optical intensity of a semiconductor laser is directly proportional to the laser current, variations in current also result in corresponding changes in intensity. The laser intensity can be then expressed as:

$$I(t) = I_0 + \Delta I\cos w_m t\# \quad (2)$$

I_0 is the laser output intensity in its unmodulated state, and ΔI denotes the amplitude of the optical intensity variation induced by the modulation.

In QEPAS, a lock-in amplifier (LIA) is employed to perform second harmonic (2f) demodulation on the weak target signal, which carries gas concentration information. This approach exploits the characteristic wavelength-dependent absorption profiles of gas molecules. When a laser is tuned to a gas absorption line and modulated sinusoidally (as described in Eq. 1), the transmitted intensity exhibits nonlinear absorption-induced distortions. These distortions generate harmonic components, with the second harmonic (2f) being particularly sensitive to the gas concentration while rejecting low-frequency noise [38–40]. This technique effectively suppresses ambient and system noise, significantly enhancing the signal-to-noise ratio (SNR). For 2f demodulation, the LIA requires a synchronous reference signal at the same frequency as the modulated target signal. This synchronization allows the LIA to selectively identify, amplify, and extract the relevant signal while

efficiently rejecting noise at other frequencies. In essence, the synchronous reference signal acts as a "key" for the LIA, unlocking the specific frequency of interest and filtering out unwanted interference. A function generator (FG) is used to modulate the laser while simultaneously generating a synchronized TTL electrical signal at the same frequency, which is directly supplied to the lock-in amplifier (LIA) as a reference signal.

In contrast, OSSD eliminates the need for an external electrical reference signal. Instead, after laser modulation, a 1:99 fiber beam splitter directs 1 % of the laser beam to a photodetector (PD). The PD captures the laser intensity signal, $I(t)$, and converts it into an electrical signal, which is then fed in real time to the LIA. As described in Eq. (2), $I(t)$ inherently contains the modulation frequency ω_m, making it a natural synchronous reference signal.

To precisely extract and amplify the desired frequency component ω_m from I(t), the LIA employs phase-sensitive detection. A stable sinusoidal oscillation signal is generated by the internal phase-locked loop (PLL) of the lock-in amplifier (LIA), forming the basis for its phase-sensitive detection. This signal can be expressed as:

$$R_{LIA}(t) = R_0 \sin w_{LIA} t\# \tag{3}$$

where R_0 represents the amplitude of the oscillation signal, and w_{LIA} is its angular frequency. The PLL circuit of the LIA ensures that both the frequency and phase of this internal oscillation signal remain precisely locked to the external reference signal. This synchronization is essential for accurate signal extraction. A key step in the LIA's operation is mixing the oscillation signal, $R_{LIA}(t)$), with the input signal—in this case, the modulated optical intensity signal $I(t)$, acquired by the PD and converted into an electrical signal.

This mixing process involves multiplying the two signals, yielding the following mixed signal:

$$S(t) = I_0 R_0 \sin(w_{LIA} t) + \frac{\Delta I R_0}{2}[\sin(w_m + w_{LIA})t - \sin(w_m - w_{LIA})t]\# \tag{4}$$

This mixed signal comprises multiple frequency components, including the sum and difference of the reference frequency w_{LIA} and the modulation frequency w_m. To extract the desired frequency component, the mixed signal is then passed through a low-pass filter. This filter efficiently attenuates high-frequency components, allowing only the low-frequency components to pass through:

$$S_{LPF}(t) = -\frac{\Delta I R_0}{2}\sin(w_m - w_{LIA})t\# \tag{5}$$

The low-pass filtered signal, $S_{LPF}(t)$ plays a critical role in the LIA's operation. It contains a component at the difference frequency $w_m - w_{LIA}$ and, and its amplitude peaks when the reference angular frequency w_{LIA} matches the modulation frequency w_m.

By sweeping the reference angular frequency w_{LIA} and monitoring the DC component of $S_{LPF}(t)$, the LIA can identify the frequency at which the signal reaches its maximum. This allows for precise determination of the modulation frequency ω_m (or equivalently, f_m). Importantly, the LIA does not measure the modulation frequency directly; rather, it detects the peak response, ensuring that the reference and modulation frequencies are perfectly synchronized for optimal signal extraction.

3. Experimental setup

Fig. 1 illustrates the system configuration of the QEPAS sensor based on the OSSD method. Specifically, it provides a detailed schematic of OSSD approach, in which a 1:99 beam splitter (BS) divides the modulated laser source into two beams: a strong beam (99 %) utilized for gas sensing and a weak beam (1 %) serving as the synchronous signal. The 99 % beam is directed through a fiber focuser with a 10 mm focal length to interact with gas molecules in the ADM generating sound waves. To prevent photothermal noise, the laser is carefully aligned to pass through the gap between the prongs of the quartz tuning fork (QTF)

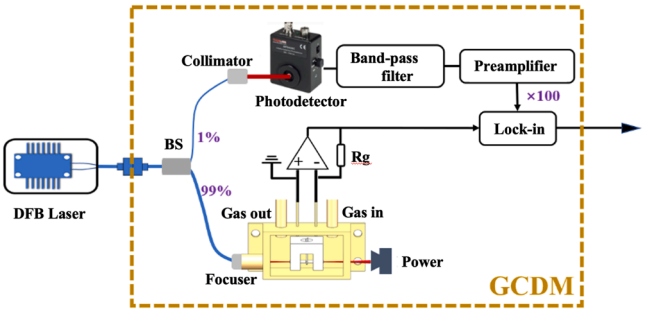

Fig. 1. Detailed schematic configuration of the QEPAS sensor based on the OSSD method.

without making contact and avoid generation of photothermal noise. The resulting sound waves induce mechanical vibrations in the QTF, which converts them into an electrical signal. This signal is amplified by a transimpedance amplifier and subsequently demodulated by a lock-in amplifier (Stanford Research Systems, Inc., SR830). A power meter is positioned behind the ADM for alignment purpose. The 1 % weak laser beam is detected by a PD (THORLABS, PDA 10CF-EC), which converts the optical signal into a corresponding electrical signal. To minimize noise interference, a band-pass filter is employed, followed by a pre-amplifier that amplifies the filtered signal. The commercial standard QTF employed in the sensor has a resonant frequency (f_0) of is 32.76 KHz, resulting in a modulation frequency of $f_0/2 = 16.38$ kHz. Consequently, the bandpass filter is configured with a bandwidth of 10K-30K to effectively isolate the target signal. The electrical signal is amplified by a factor of 100 using the preamplifier, after which a phase-locked loop stabilizes the amplified signal. This stabilized signal is then transmitted to the synchronous port of the LIA, where it serves as a reference for demodulating the electrical output from the ADM. For simplicity, the apparatus depicted in Fig. 1 is referred to as the gas concentration detection module (GCDM).

In conventional QEPAS technology, the LIA transmits the final QEPAS signal to a computer via a cable for data display and recording. However, in complex environments, computers are susceptible to damage, resulting in unnecessary financial losses. To mitigate this issue, a wireless communication module (WCM) is integrated into the GCDM backend, enabling real-time, long-range data transmission. This allows the computer to be safely positioned away from the measurement point. The WCM, based on Zigbee technology, offers several advantages, including low cost, minimal power consumption, and an operational lifespan of several months using standard AA batteries. It supports a Mesh Network, enabling the extension of communication range through relay transmission between multiple nodes. In this configuration, the theoretical communication distance can be extended indefinitely, as long as the distance between nodes remains within the communication range of a single node. The specific implementation scheme is illustrated in Fig. 2. After demodulation by the LIA, the signal is transmitted to the wireless transmission module (WTM), which relays the data to a wireless receiving module (WRM). The WRM then forwards the processed data to the computer. In practical applications, gas concentration detection and recording are typically required at regular intervals. To optimize resource allocation, a transpose switch, integrated with the lasers module, enables time-multiplexed measurements across multiple regions —especially valuable when working with high-cost laser sources. This approach facilitates time-sharing remote synchronous measurement. The collected data from each region is first sent to the WTM, which transmits it to a wireless repeater module (WREP), before final delivery to the computer for processing and analysis.

To assess the practical feasibility of the system, particularly its performance in complex environments, we conducted CH_4 monitoring in sewer environments. A continuous wave DFB laser with a center wavelength of 1.65 μm (NTT Electronics, NLK1U5EAAA) was used as the

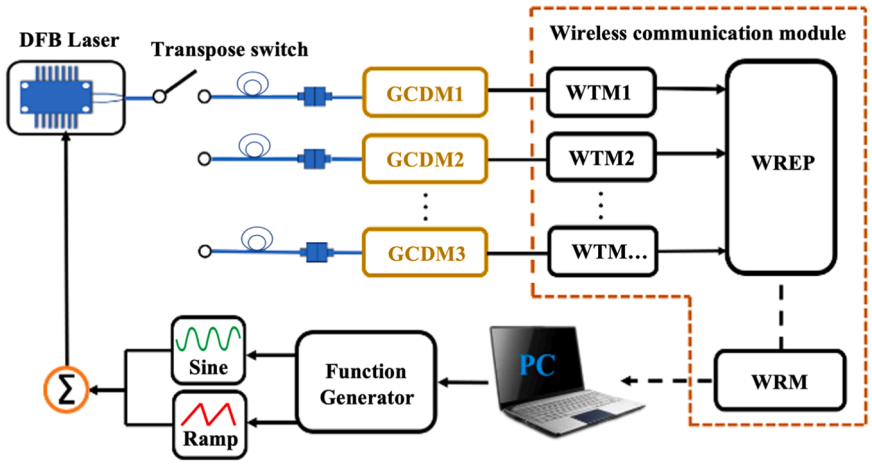

Fig. 2. Schematic diagram of time-sharing remote synchronous QEPAS sensing system based on the OSSD.

excitation light source for CH_4 detection. For laser wavelength modulation and enhanced sensitivity through 2*f* detection, a computer-controlled function generator FG (Tektronix, AFG3102C) produced a sinusoidal signal at half the QTF frequency (16.38 kHz). The laser temperature was set to 16.38 °C, and the same FG also generated a triangular wave to scan the laser current from 120 mA to 160 mA, the laser output wavelength ranged from 6046.22 cm^{-1} to 6047.78 cm^{-1}, ensuring that the laser fully covered the CH_4 absorption line centered at 6046.96 cm^{-1}, free from interference from other gas species that can be present in a sewer environment. The sinusoidal and triangular signals were combined using an adder to drive the laser current. At 139.2 mA, the laser output power was measured at 20.3, which implies that 1 % of the synchronous signal optical power is 0.23 mW. After transmission through 2 km, 5 km, and 10 km of fiber, the retained optical power can reach 0.21 mW, 0.183 mW, and 0.146 mW, respectively. Therefore, even at distances of 10 km or more, the system maintains excellent performance.

To validate the system's practicality, time-resolved CH_4 concentration measurements were performed at two campus sewer wells. Specifically, long-distance optical fibers were employed to measure CH_4 levels at 200 m from the laser source, corresponding to the research institute's sewer well, and at 1000 m, corresponding to the canteen sewer well. A transpose switch at the laser-fiber interface enabled remote, time-shared, and synchronous acquisition of CH_4 concentration data from both locations. The acquired data was then transmitted via WCM to a computer for processing and analysis

Fig. 3(a) and (b) illustrate the CAD model and the photograph of a compact, fiber-coupled ADM, co-developed by Achray Photonics, Inc. (Ottawa, QC, Canada) and Rice University (Houston, TX, USA), for target gas detection [24,41,42]. The ADM features a telecom-style, butterfly-packaged shell, constructed from a nickel-iron alloy with a thin gold coating to enhance durability and performance. To achieve higher detection sensitivity compared to conventional bare QTF-based QEPAS sensors, the ADM employs an on-beam resonator configuration. The resonator, measuring 4.4 mm in length with an inner diameter of 0.6 mm, is held in place by a 3D-printed bracket, ensuring precise alignment with the QTF. A single-mode fiber, equipped with a lens termination, is mounted on the right side of the ADM to couple the laser light into the module and through the QTF prongs. On the left side of the ADM, a 6.5 mm calcium fluoride window, facilitates optical path alignment. Additionally, gas inlet and outlet ports are integrated into the side of the ADM allowing for real-time gas exchange.

With compact dimensions of 21 × 12.7 × 8.5 mm^3, the ADM is lightweight, highly stable, and easily deployable, making it particularly well-suited for real-time CH_4 detection in sewer environments. During system setup, the ADM was sealed with a matching lid, and calibrated using known CH_4 concentrations, which were introduced through the inlet and outlet ports. For in-situ CH_4 measurements in sewers environments, the ADM was operated in an open configuration, as shown in Fig. 3(b).

To ensure reliable operation of the electronics under challenging conditions, we implemented several protective measures: Robust enclosure: the LIA is housed in a weatherproof, corrosion-resistant enclosure with sealed gaskets to prevent moisture and dust ingress; Temperature Control: Passive or active cooling/heating systems maintaining optimal operating temperatures; Vibration Resistance: Components are mounted on shock-absorbing materials to withstand mechanical stress; Electrical Protection: EMI shielding and surge protection safeguarding against electrical interference; Maintenance and Monitoring: Regular inspections and remote monitoring ensuring early detection of potential issues.

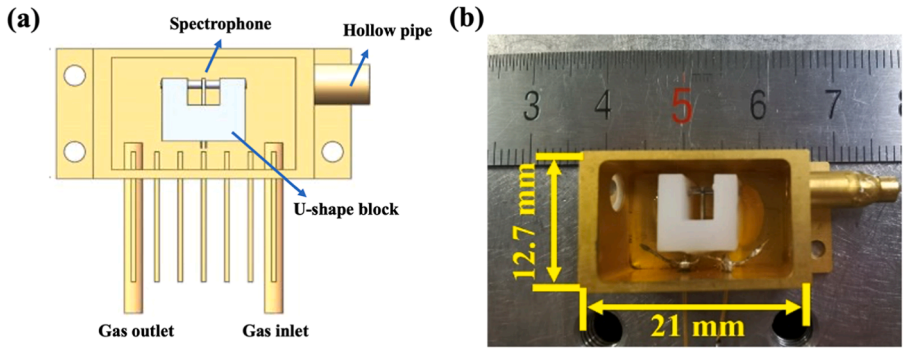

Fig. 3. (a) CAD image of the fiber-coupled ADM. (b) photograph of the fiber-coupled ADM.

4. Experimental results and discussion

4.1. Performance evaluation of the OSSD

As a high-frequency optical electromagnetic wave (ranging from 10^{13} to 10^{15} Hz [43]), laser light serves as an ideal carrier for information transmission. Light waves offer several advantages, including high propagation speed, large data capacity, ease of manipulation through optical systems, and multiple transmission modalities. Laser modulation involves encoding low-frequency information onto the laser beam, while demodulation is the inverse process—retrieving the embedded information from the carrier signal. Since demodulation typically requires a reference to the original modulating signal, ensuring the integrity of this signal is crucial for accurate data extraction. To assess the stability, accuracy, and feasibility of the OSSD, a 1000-meter optical fiber was used to transmit the laser. After transmission, a 1:99 beam splitter was used to separate the laser into two beams: a strong 99 % beam, used for gas sensing; a weak 1 % beam, serving as the synchronous reference signal. To ensure effective synchronous demodulation, it is critical to verify that the 1 % weak beam, after modulation and beam splitting, retains high fidelity and accurately preserves the modulation information. Additionally, the low-frequency signal embedded in the laser must remain robust, unaffected by factors such as fiber transmission over long distances (1000 m), variations in light intensity, or optical system transformations.

In the QEPAS system, wavelength modulation of the laser is achieved by simultaneously applying frequency modulation and current scanning using a FG. The accuracy of the optical synchronization signal can be verified by comparing the FG output with the laser-carried signal. For ease of observation, in this section, the FG generates a sinusoidal wave with a period of 1-second period and a modulation depth of 15 mA, corresponding to the frequency modulation, and a triangular wave with a 7-second period and a current scanning range of 70 mA −110 mA, corresponding to the current scan. The laser intensity signal, as detected by the PD, and the FG output were simultaneously recorded using an oscilloscope (Tektronix DPO 2024) for real-time observation. Additionally, both signals were acquired in real-time using a data acquisition card (DAQ, NI USB-6361) for further analysis.

Fig. 4 presents the results of the verification experiment. Fig. 4(a) and (b) show the sinusoidal and triangular wave signals, respectively, as acquired by the DAQ from the FG. Fig. 4(c) displays the optical intensity signal detected by the PD from the 1 % weak laser beam. The results indicate the PD-detected optical intensity signal exhibits a 7-second period triangular wave overlaid with a 1-second period sinusoidal wave, where each 7-s scan cycle contains seven sinusoidal waveforms. Notably, the measured frequencies precisely match those of the superimposed FG output, confirming that the OSSD system effectively carries the modulation signal and provides an accurate synchronization signal over long-distance optical fiber transmission. From this, the following conclusions can be drawn: (1) Optical power loss does not affect the transmission of the synchronization signal; (2) Long-distance optical fiber transmission does not introduce frequency distortion in either the modulation or scan signals; (3) Long optical fiber transmission does not affect the superposition of the modulation and scan signals.

In this experiment, the DAQ directly acquired the PD's output signal without applying any filtering or amplification. However, in real-world complex environments, optical power attenuation can lead to synchronization signal distortion, while unwanted signal mixing may interfere with the demodulation of the photoacoustic signal. Therefore, although Fig. 4 confirms the expected experimental results, the use of a bandpass filter and preamplifier is essential in the OSSD system to ensure robust synchronization signal integrity and interference-free demodulation under practical operating conditions.

To systematically validate the feasibility of the OSSD technique, CH_4 concentration measurements were conducted using both conventional electrical signal demodulation techniques and the novel OSSD method on a standard gas mixture of 1 % CH_4 in N_2 matrix. Experiments were performed under ambient temperature and pressure conditions to simulate actual sewer environments. A pressure monitor (MKS Instruments Inc., Andover, MA, USA) maintained atmospheric pressure in the gas flow path, while a flow meter (Alicat Scientific, Inc., M-500SCCM-D/5 M) continuously monitored and stabilized the flow rate at 100 sccm.

As previously described, 2*f* demodulation was achieved by setting the frequency of the sinusoidal modulation signal from the FG to half the QTF resonance frequency, specifically 16.38 kHz, with a modulation amplitude of 10 mA. Simultaneously, a triangular wave scanning signal from the FG varied from 120 mA to 160 mA to scan the laser emission wavelength across the target absorption line. To ensure accurate and comprehensive data, the scanning frequency was set to 20 mHz. As shown in Fig. 5, the signal amplitudes and second harmonic line shapes detected at the same CH4 concentration exhibit strong agreement

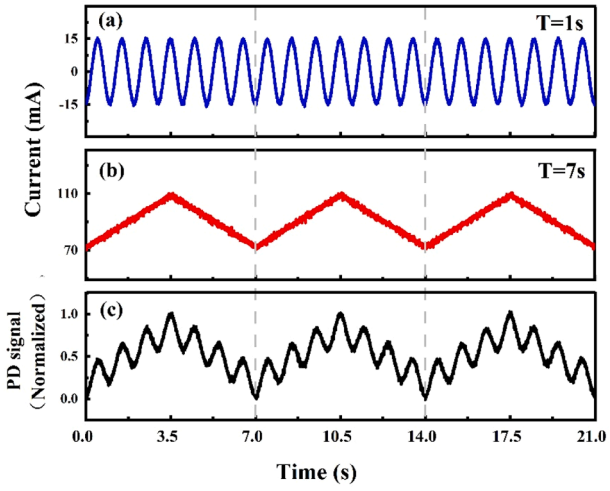

Fig. 4. (a) 1 s period sine signal generated by FG. (b) 7 s period triangular wave signal generated by FG. (c) Normalized signal of the 1 % weak laser beam, measured by the photodetector (PD) after transmission through 1000 m of optical fiber, demonstrating the preservation of the two superimposed modulation signals.

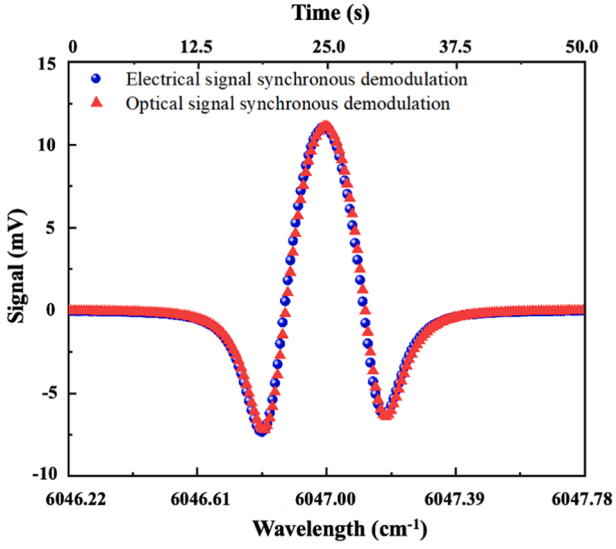

Fig. 5. Comparison of 1 % CH_4/N_2 concentration measurements using conventional electrical signal demodulation technology and the proposed OSSD method.

between the traditional synchronous demodulation method (blue data points) and the novel OSSD technique (red data points). This confirms the accuracy and reliability of the OSSD technique, demonstrating its viability as an alternative to conventional demodulation methods.

4.1.1. Performance optimization of CH_4 sensor

Given CH_4's relatively low relaxation rate, it is common practice to introduce gases with higher relaxation rates to enhance the photoacoustic signal and improve detection sensitivity. Water vapor, commonly used for this purpose, has a concentration-dependent amplifying effect on the CH_4 photoacoustic response. However, its catalytic enhancement saturates at concentration above 1 % [3], meaning further increases do not provide additional signal amplification. As a result of optimization, CH_4 detection in high-humidity sewer environments remains largely unaffected by variations in moisture content. A silicone hollow fiber membrane device (PermSelect, PDMSXA-2500) was employed as a humidifier to precisely regulate the vapor concentration in the gas line at 2.5 %, with the actual concentration accurately measured using a chilled mirror dew point meter (DewMaster, DM-C1). Fig. 6(a) compares the photoacoustic signals of a a 1 % CH_4/N_2 mixture before and after humidification. The red line represents the 2 *f* signal of dry 1 % CH_4/N_2, while the blue line corresponds to the 2 *f* signal with 2.5 % water vapor. As shown, the peak amplitude increases from 11 mV to 29 mV, indicating that water vapor enhances the CH_4 photoacoustic signal by a factor of 2.6.

In wavelength modulation technology, modulation depth is a critical parameter that directly influences the amplitude of the 2 *f* signal. Optimizing this parameter enhances the CH_4 photoacoustic signal, improving detection sensitivity. As shown in Fig. 6(b), the results indicate that a modulation depth of 12 mA provides the optimal signal amplitude for of CH_4 detection.

To evaluate the performance of the CH_4 sensor, measurements were conducted for CH_4 concentrations ranging from 200 ppm to 1000 ppm. A gas diluter (MCQ, GB-103) was used to generate the desired different H_4 concentration by precisely mixing high-purity nitrogen with a 1 % CH_4/N_2 certified mixture. The corresponding photoacoustic signals are shown in Fig. 7. A linear fit of the data yielded an R-square value of 0.999, demonstrating the sensor's excellent linear response to CH_4 concentration.

All experimental measurements were conducted with a 300 ms time constant and a 12 dB/oct filter slope on the LIA. Analysis of the CH_4 signal at 1 % concentration yielded a 1σ noise level of 4.8 μV and a minimum detection limit of 445 ppb. The corresponding normalized noise equivalent absorption (NNEA) coefficient was determined to be 5.25×10^{-9} cm^{-1}·W/$Hz^{1/2}$.

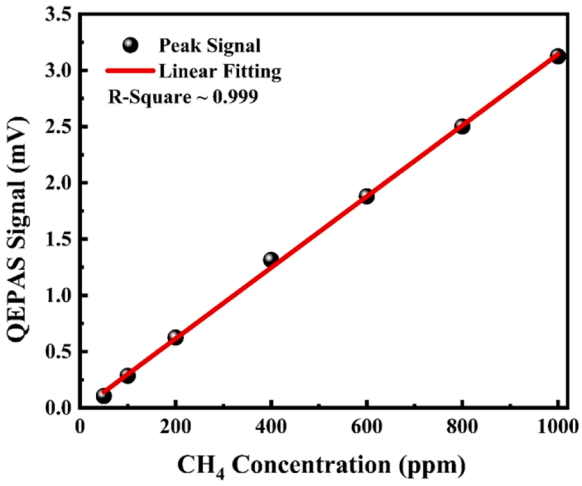

Fig. 7. The linear relationship between QEPAS signal and concentration of CH_4 QEPAS sensor based on the OSSD.

4.2. Remote synchronous detection of CH_4 concentration in sewers

The QEPAS CH_4 sensor utilizing the OSSD technique was deployed for time-sharing CH_4 concentration measurements in two sewers locations on the Shanxi university campus. Location 1 corresponds to a sewer near the Institute of Laser Spectroscopy, situated 200 m from the laser source, while Location 2 is a sewer adjacent to the campus canteen, located 1000 m away. Two identical ADMs were installed at each site via 200-meter and 1000-meter optical fibers, respectively. A 6 mm outer diameter Teflon tube was used to extract gas from the sewers, with a micropore filter removing dust and soot particles. To ensure a stable and saturated water vapor concentration in the detection path, the filtered gas was humidified by a dedicated humidifier before being pumped into the ADM by a vacuum pump (Oerlikon Leybold Vacuum Inc., Cologne, Germany). The ADM's output signal was transmitted to the LIA, where

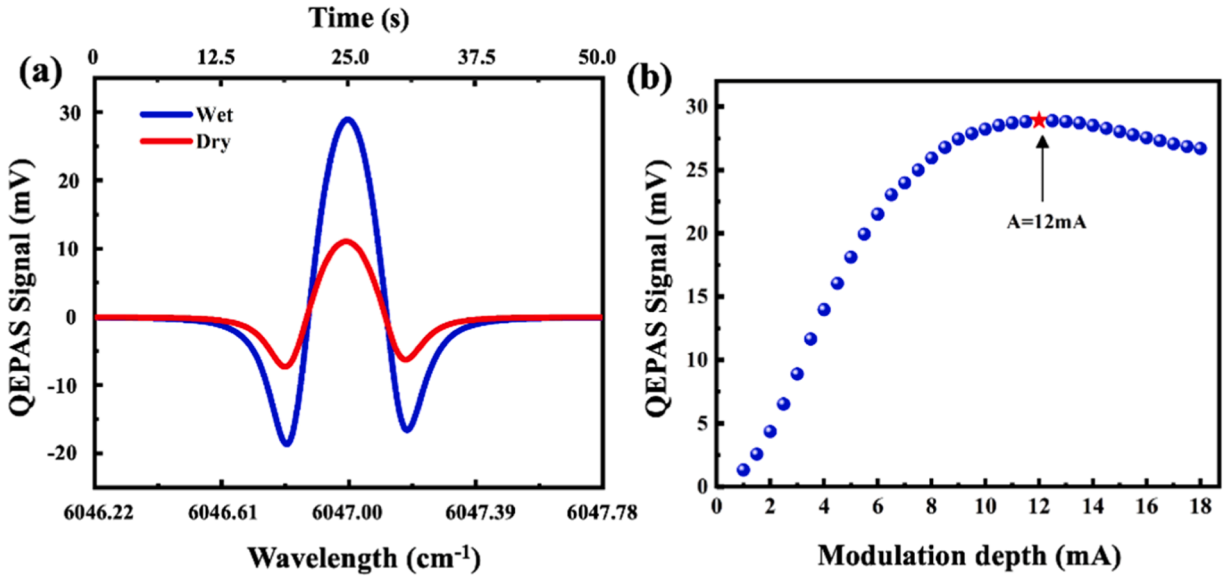

Fig. 6. (a) Comparison of the photoacoustic signal of a 1 % CH_4/N_2 mixture before and after humidification. The red line represents the signal in dry conditions, while the blue line shows the signal after adding of 2.5 % water vapor. (b) Optimization of modulation depth for a 1 % CH_4/N_2 mixture.

the CH_4 2*f* photoacoustic signal was demodulated using the OSSD technique. The processed data was then sent via the WCM to the computer for the real-time CH_4concentration analysis. Fig. 8 presents in-situ CH_4 concentration measurements in the sewers at Location 1 and Location 2 over a 14-hour period. CH_4 concentration at Location 1 was monitored from 08:00–22:00, while measurements at Location 2 were conducted from 08:10–22:10. A transfer switch was used to alternate measurements between the two locations every 10 minutes, enabling time-shared detection. The measurements were performed on July 17. On this day, the ambient temperature started at 22°C at 08:00, rose to a peak of 34°C around 14:30, and then gradually decreased to 25°C by 22:00. The experimental results in Fig. 8(a) and (b) were obtained by averaging the data over ten-minute intervals for each location.

Fig. 8(a) presents CH_4 concentration measurements in the sewer at Location 1. The primary source of organic matter in this sewer is waste discharged from toilets. Due to the presence of a drain cover, atmospheric wind can enter the sewer, leading to high oxygen levels and a relatively slow decomposition rate of organic matter. As a result, the CH_4 concentration remains low, generally below 400 ppm, and the detection data appears irregular. Despite these fluctuations, a clear pattern emerges: between 10:00 and 18:00, increased environmental temperatures and human activity accelerate the fermentation of organic matter, leading to a rise in CH_4 concentration. Conversely, after 18:00, as ambient temperatures drop, fermentation slows down, resulting in a gradual decline in CH_4 levels.

The CH_4 concentration measurements in sewer at Location 2 are shown in Fig. 8(b). The data clearly indicates that CH_4 levels increase during three distinct time periods: 08:10–10:10, 12:10–15:10, and 17:10–19:10, with peak concentrations of 360 ppm, 849 ppm, and 430 ppm, respectively. These fluctuations correlate with meal preparation times in the canteen, where breakfast, lunch, and dinner services start at 07:00, 11:00, and 17:00, respectively. During these periods, the discharge of organic waste from the kitchen and dishwashing room increases significantly, leading to a higher concentration of organic matter in the sewer and subsequently elevated CH_4 levels. Notably, between 12:10 and 15:10, CH_4 concentrations rise more sharply compared to the other periods. This can be attributed to higher ambient temperatures, which enhance the fermentation efficiency of organic matter, accelerating CH_4 production. In contrast, during the 08:10–10:10 and 17:10–19:10 periods, CH_4 concentrations are lower due to cooler temperatures, which slow down fermentation rates. Between 10:10–12:10, 15:10–17:10, and 20:10–22:10, CH_4 levels decline as the amount of organic matter in the sewer decreases, following a reduction in wastewater discharge from the canteen. These experimental results align with expected CH_4 production patterns in sewers, further validating the performance of the QEPAS CH_4 sensor based on the OSSD technique.

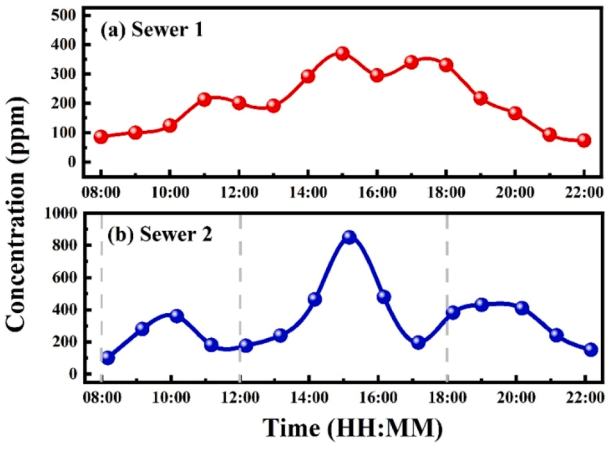

Fig. 8. Real-time CH_4 concentration monitoring at two sewer locations. (a) CH_4 concentration in Location 1 sewer. (b) CH_4 concentration in Location 2 sewer.

To further explore the effects of different gases on the photoacoustic signal, we investigated the absorption spectra of CH_4, H_2O, and CO_2 using the HITRAN database. H_2O and CO_2 are commonly found in sewer emissions, and their concentration levels can significantly affect the measurement accuracy of the photoacoustic signal. Therefore, we set the concentrations of these two gases at 1 %, while the concentration of CH_4 was set at 1 ppm. Fig. 9 presents the absorption spectra within the wavelength range of 6046.3 cm^{-1} to 6047.6 cm^{-1}, which includes a significant absorption peak for CH_4 at 6046.96 cm^{-1}. Based on the characteristics of the absorption spectra, CH_4 molecules exhibit strong absorption in this wavelength range, while the absorption features of H_2O and CO_2 are located at nearby wavelengths, which could potentially cause some degree of interference. However, the data shown in the figure indicate that, despite the presence of H_2O and CO_2 absorption, there is no significant interference with the main absorption peak of methane. Therefore, we can reasonably conclude that under the experimental conditions, the signal of CH_4 is not significantly affected by other gases, which supports our detection results.

5. Conclusions

In this study, we developed and validated a novel Optical Synchronous Signal Demodulation (OSSD) method for gas detection in complex environments using Quartz-Enhanced Photoacoustic Spectroscopy (QEPAS). This technique effectively overcomes the limitations of traditional electrical signal transmission, including signal distortion, high costs, and distance constraints. By utilizing the modulated optical signal as a synchronous reference, OSSD enables robust and precise gas concentration demodulation through a lock-in amplifier.

The feasibility of OSSD was confirmed by comparing the modulated signal carried by the laser with that generated by a function generator, as well as by analyzing the second harmonic signals of a standard 1 % CH_4/N_2 mixture. A QEPAS-based CH_4 sensor integrated with OSSD was deployed for real-time CH_4 monitoring in two campus sewer locations over a 14-hour period. The system utilized 200-meter and 1,000-meter optical fibers to enable in-situ CH_4 detection. A transfer switch facilitated time-sharing measurements at both locations.

The QEPAS CH_4 sensor with OSSD achieved a minimum detection limit of 445 ppb, and the Normalized Noise Equivalent Absorption (NNEA) coefficient was determined to be 5.25×10^{-9} $cm^{-1} \cdot W/Hz^{1}/^{2}$. These results confirm that OSSD-QEPAS is a viable, cost-effective, and scalable solution for long-range gas sensing applications.

Looking forward, OSSD-based multi-gas time-division remote sensing will be explored for applications in oil and gas exploration,

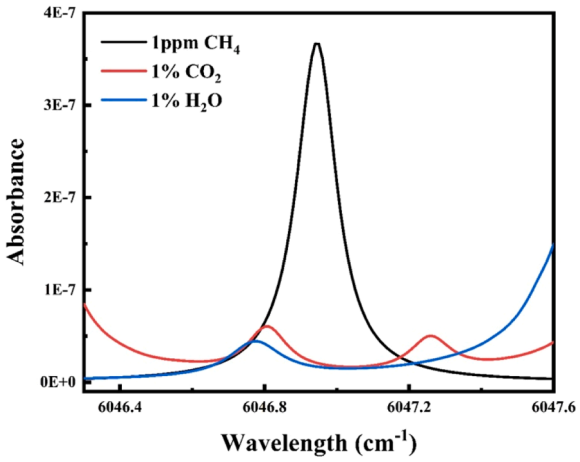

Fig. 9. CH_4, H_2O and CO_2 absorbance spectra in the infrared region provided by the HITRAN database in the spectral range of 6046.3 cm^{-1} and 6047.6 cm^{-1}.

industrial monitoring of hazardous gas emissions, and environmental safety assessments.

CRediT authorship contribution statement

Spagnolo Vincenzo: Writing – review & editing, Supervision, Project administration, Methodology, Funding acquisition, Conceptualization. **Dong Lei:** Writing – review & editing, Supervision, Project administration, Methodology, Funding acquisition, Conceptualization. **Wu Hongpeng:** Writing – review & editing, Supervision, Methodology, Conceptualization. **Qiao Lijun:** Investigation, Data curation, Conceptualization. **Zhang Mingjiang:** Writing – review & editing, Supervision, Methodology, Conceptualization. **Wei Tingting:** Writing – original draft, Data curation, Conceptualization. **Sun Bo:** Writing – original draft, Methodology, Investigation, Conceptualization. **Patimisco Pietro:** Writing – review & editing, Methodology, Conceptualization. **Sampaolo Angelo:** Writing – review & editing, Methodology, Conceptualization. **Ma Zhe:** Writing – original draft, Methodology, Data curation, Conceptualization.

Declaration of Competing Interest

The authors declare that they have no known competing financial interests or personal relationships that could have appeared to influence the work reported in this paper.

Acknowledgments

The project is supported by National Natural Science Foundation of China (NSFC) [grant numbers 62475137, 62235010, 62105252]; The Shanxi Science Fund for Distinguished Young Scholars (20210302121003); National Key Research and Development Program of China (2023YFF0715700) and Natural Science Foundation of China (U23A20375); The authors from Dipartimento Interateneo di Fisica di Bari acknowledge financial support from the Italian Minister of University project– Dipartimenti di Eccellenza 2023–2027 – Quantum Sensing and Modelling for One-Health (QuaSiModO) and THORLABS GmbH within the PolySenSe joint research laboratory;

Data Availability

Data will be made available on request.

References

[1] M. Olivieri, G. Menduni, M. Giglio, A. Sampaolo, P. Patimisco, H. Wu, L. Dong, V. Spagnolo, Characterization of H_2S QEPAS detection in methane-based gas leaks dispersed into environment, Photoacoustics 29 (2023) 100438.
[2] K. Kinjalk, F. Paciolla, B. Sun, A. Zifarelli, G. Menduni, M. Giglio, H. Wu, L. Dong, D. Ayache, D. Pinto, A. Vicet, A. Baranov, P. Patimisco, A. Sampaolo, V. Spagnolo, Highly selective and sensitive detection of volatile organic compounds using long wavelength InAs-based quantum cascade lasers through quartz-enhanced photoacoustic spectroscopy, Appl. Phys. Rev. 11 (2024) 021427.
[3] M. Giglio, A. Zifarelli, A. Sampaolo, G. Menduni, A. Elefante, R. Blanchard, C. Pfluegl, M.F. Witinski, D. Vakhshoori, H. Wu, V.M.N. Passaro, P. Patimisco, F. K. Tittel, L. Dong, V. Spagnolo, Broadband detection of methane and nitrous oxide using a distributed feedback quantum cascade laser array and quartz-enhanced photoacoustic sensing, Photoacoustics 17 (2020) 100159.
[4] B. Sun, A. Zifarelli, H. Wu, S.Dello Russo, S. Li, P. Patimisco, L. Dong, V. Spagnolo, Mid-infrared quartz-enhanced photoacoustic sensor for ppb-level CO detection in a SF_6 gas matrix exploiting a t-grooved quartz tuning fork, Anal. Chem. 92 (2020) 13922–13929.
[5] V. Spagnolo, P. Patimisco, S. Borri, G. Scamarcio, B.E. Bernacki, J. Kriesel, Part-per-trillion level SF_6 detection using a quartz enhanced photoacoustic spectroscopy-based sensor with single-mode fiber-coupled quantum cascade laser excitation, Opt. Lett. 37 (2012) 4461–4463.
[6] S. Khandaker, N. Shaipuzaman, M.M. Hasan, M.A. Mohd Aspar, H. Manap, A comprehensive review of state-of-the-art optical methods for methane gas detection, Pertanika J. Sci. Technol. 32 (2024) 5032.
[7] R. Levy, M. Duquesnoy, J. Melkonian, M. Raybaut, G. Aoust, New signal processing for fast and precise QEPAS measurements, IEEE Trans. Ultrason. Ferroelectr. Freq. Control 67 (6) (2020) 1230–1235.
[8] J. Zhao, H. Zhang, Y. Fu, L. Qin, J. Shi, Y. Zhao, Integrated multiexcitation dual-spectroscopy detection technique based on QEPTS and QEPAS, IEEE Sens. J. 24 (2024) 16130–16136.
[9] H. Hodara, Performance trade-off of coaxial and fiberoptic cables, Fiber Integr. Opt. 5 (2) (1985) 203–237.
[10] U. Stanley, V.M. Olu, C. Ochonogor, P. Amaize, A. Francis, Experimental analysis of cable distance effect on signal attenuation in single and multimode fiber optics, Int. J. Electr. Comput. Eng. 8 (2018) 1577.
[11] R. Watanabe, T. Kondo, T. Watanabe, Low-loss coaxial cable with highly foamed insulator, Fujikura Tech. Rev. 37 (2008) 43.
[12] S. Hengoju, O. Shvydkiv, M. Tovar, M. Roth, M.A. Rosenbaum, Advantages of optical fibers for facile and enhanced detection in droplet microfluidics, Biosens. Bioelectron. 200 (2022) 113910.
[13] Y. Koike, K. Koike, Progress in low-loss and high-bandwidth plastic optical fibers, J. Polym. Sci. Part B: Polym. Phys. 49 (2011) 2–17.
[14] G. Wu, J. Xing, Z. Gong, J. Ma, Y. Fan, X. Wu, W. Peng, Q. Yu, L. Mei, Single fiber-type double cavity enhanced photoacoustic spectroscopy sensor for trace methane sensing, J. Light. Technol. 42 (2024) 3393–3398.
[15] X. Yin, H. Wu, L. Dong, B. Li, W. Ma, L. Zhang, W. Yin, L. Xiao, S. Jia, F.K. Tittel, ppb-Level SO_2 photoacoustic sensors with a suppressed absorption−desorption effect by using a 7.41 μm external-cavity quantum cascade laser, ACS Sens 5 (2020) 549–556.
[16] C. Zhang, Y. He, S. Qiao, Y. Liu, Y. Ma, High-sensitivity trace gas detection based on differential Helmholtz photoacoustic cell with dense spot pattern, Photoacoustics 38 (2024) 100634.
[17] C. Feng, B. Li, Y. Jing, J. Wang, P. Patimisco, V. Spagnolo, L. Dong, H. Wu, Enrichment enhanced photoacoustic spectroscopy based on vertical graphene, Sens. Actuators B: Chem. 145 (2024) 136204.
[18] B. Li, H. Wu, C. Feng, J. Wang, S. Jia, P. Zheng, L. Dong, Photoacoustic heterodyne CO Sensor for Rapid Detection of CO Impurities in Hydrogen, Anal. Chem. 96 (1) (2023) 547–553.
[19] H. Wu, L. Dong, H. Zheng, Y. Yu, W. Ma, L. Zhang, W. Yin, L. Xiao, S. Jia, F. K. Tittel, Beat frequency quartz-enhanced photoacoustic spectroscopy for fast and calibration-free continuous trace-gas monitoring, Nat. Commun. 8 (1) (2017) 15331.
[20] B. Sun, P. Patimisco, A. Sampaolo, A. Zifarelli, V. Spagnolo, H. Wu, L. Dong, Light-induced thermoelastic sensor for ppb-level H_2S detection in a SF_6 gas matrices exploiting a mini-multi-pass cell and quartz tuning fork photodetector, Photoacoustics 33 (2023) 100553.
[21] J. Wang, H. Wu, A. Sampaolo, P. Patimisco, V. Spagnolo, S. Jia, L. Dong, Quartz-enhanced multiheterodyne resonant photoacoustic spectroscopy, Light.: Sci. Appl. 13 (2024) 77.
[22] P. Breitegger, B. Schweighofer, H. Wegleiter, M. Knoll, B. Lang, A. Bergmann, Towards low-cost QEPAS sensors for nitrogen dioxide detection, Photoacoustics 18 (2020) 100169.
[23] A. Sampaolo, P. Patimisco, M. Giglio, A. Zifarelli, H. Wu, L. Dong, V. Spagnolo, Quartz-enhanced photoacoustic spectroscopy for multi-gas detection: a review, Anal. Chim. Acta 1202 (2021) 338894.
[24] P. Patimisco, A. Sampaolo, H. Zheng, L. Dong, F.K. Tittel, V. Spagnolo, Quartz−enhanced photoacoustic spectrophones exploiting custom tuning forks: a review, Adv. Phys.: X. 2 (2017) 169–187.
[25] A. Sampaolo, S. Csutak, P. Patimisco, M. Giglio, G. Menduni, V. Passaro, F.K. Tittel, M. Deffenbaugh, V. Spagnolo, Methane, ethane and propane detection using a compact quartz enhanced photoacoustic sensors and a single interband cascade laser, Sens. Actuators B Chem. 282 (2019) 952–960.
[26] T. Wei, A. Zifarelli, S.Dello Russo, H. Wu, G. Menduni, P. Patimisco, A. Sampaolo, V. Spagnolo, L. Dong, High and flat spectral responsivity of quartz tuning fork used as infrared photodetector in tunable diode laser spectroscopy, Appl. Phys. Rev. 8 (4) (2021) 041409.
[27] R. Wang, S. Qiao, Y. He, Y. Ma, Highly sensitive laser spectroscopy sensing based on a novel four-prong quartz tuning fork, Opto-Electron. Adv. 8 (2025) 240275.
[28] Y. Ma, S. Qiao, R. Wang, Y. He, C. Fang, T. Liang, A novel tapered quartz tuning fork-based laser spectroscopy sensing, Appl. Phys. Rev. 11 (2024) 041412.
[29] Y. Liu, S. Qiao, C. Fang, Y. He, H. Sun, J. Liu, Y. Ma, A highly sensitive LITES sensor based on a multi-pass cell with dense spot pattern and a novel quartz tuning fork with low frequency, Opto-Electron. Adv. 7 (3) (2024) 230230.
[30] G. Jiang, O. Gutierrez, K.R. Sharma, Z. Yuan, Effects of nitrite concentration and exposure time on sulfide and methane production sewer systems, Water Res. 44 (2010) 4241–4251.
[31] C. Liu, G. Wang, C. Zhang, P. Patimisco, R. Cui, C. Feng, A. Sampaolo, V. Spagnolo, L. Dong, H. Wu, End-to-end methane gas detection algorithm based on transformer and multi-layer perceptron, Opt. Express 32 (2024) 98.
[32] R.V. Matos, F. Ferreira, C. Gil, J. Saldanha Mato, Understanding the effect of ventilation, intermittent pumping and seasonality in hydrogen sulfide and methane concentrations in a coastal sewerage system, Environ. Sci. Pollut. Res. 26 (2019) 3404–3414.
[33] Z. Luo, T. Wang, H. Wen, J. Zhang, F. Cheng, J. Zhao, Q. Wang, Y. Wang, C. Liu, Explosion and flame emission spectra characteristics of CH_4-Air mixtures with CO addition, J. China Coal Soc. 44 (2019) 2016–2177.
[34] T. Aldhafeeri, M.-K. Tran, R. Vrolyk, M. Pope, M. Fowler, A review of methane gas detection sensors: Recent developments and future perspectives, Inventions 5 (3) (2020) 28.
[35] Y. Liu, K.R. Sharma, S. Murthy, I. Johnson, T. Evans, Z. Yuan, On-line monitoring of methane in sewer air, Sci. Rep. 4 (2014) 6637.

[36] H. Ma, Y. Chen, S. Qiao, Y. He, Y. Ma, A high sensitive methane QEPAS sensor based on self-designed trapezoidal-head quartz tuning fork and high power diode laser, Photoacoustics 42 (2025) 100683.
[37] C. Fang, T. Liang, S. Qiao, Y. He, Z. Shen, Y. Ma, Quartz-enhanced photoacoustic spectroscopy sensing using trapezoidal-and round-head quartz tuning forks, Opt. Lett. 49 (3) (2024) 770–773.
[38] L. Mei, S. Svanberg, Wavelength modulation spectroscopy—digital detection of gas absorption harmonics based on Fourier analysis, Appl. Opt. 54 (9) (2015) 2234–2243.
[39] A. Hangauer, J. Chen, R. Strzoda, M.C. Amann, Multi-harmonic detection in wavelength modulation spectroscopy systems, Appl. Phys. B 110 (2013) 177–185.
[40] Q. Zhang, J. Chang, F. Wang, Z. Wang, Y. Xie, W. Gong, Improvement in QEPAS system utilizing a second harmonic based wavelength calibration technique, Opt. Commun. 415 (2018) 25–30.
[41] L. Dong, J. Wright, B. Peters, B.A. Ferguson, F.K. Tittel, S. McWhorter, Compact QEPAS sensor for trace methane and ammonia detection in impure hydrogen, Appl. Phys. B 107 (2012) 459–467.
[42] A.A. Kosterev, L. Dong, D. Thomazy, F.K. Tittel, S. Overby, QEPAS for chemical analysis of multi-component gas mixtures, Appl. Phys. B 101 (2010) 649–659.
[43] M. Trtica, D. Batani, R. Redaelli, J. Limpouch, V. Kmetik, J. Ciganovic, J. Stasic, B. Gakovic, M. Momcilovic, Titanium surface modification using femtosecond laser with 1013–1015 W/cm^2 intensity in vacuum, Laser Part. Beams 31 (1) (2013) 29–36.

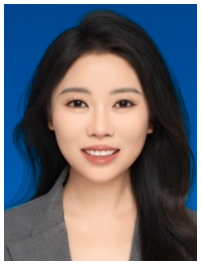

Bo Sun received her double Ph.D. degrees from Shanxi University, China, in atomic and molecular physics, and Politecnico di Bari, Italy, in industrial 4.0, in 2024. She joined Taiyuan University of Technology in 2024 as a lecturer. Her research interests include photoacoustic spectroscopy, light-induced thermoelastic spectroscopy, and optical sensors.

Tingting Wei Tingting Wei received her Ph.D. degree in atomic and molecular physics from Shanxi University, China, in 2023. Currently, she is pursuing postdoctoral research at Zhejiang University. Her main research interests include laser spectroscopy, optical sensing, and on-chip spectral sensing.

Mingjiang Zhang (Member, IEEE) received the Ph.D. degree in optics engineering from Tianjin University, Tianjin, China, in 2011. During 2015–2016, he was a Visiting Scholar with the University of Ottawa, Ottawa, ON, Canada. He is currently a Professor with the Taiyuan University of Technology, Taiyuan, China. He has coauthored more than 100 journal and conference papers. His research search interests include nonlinear dynamics of laser diodes, photonic-integrated broadband chaotic semiconductor laser, optical fiber sensing, and microwave photonics.

Lijun Qiao received the Ph.D. degree in microelectronics and solid electronics from the Institute of Semiconductors, Chinese Academy of Sciences, Beijing, China, in 2017. She is currently an Associate Professor with the College of Physics and Optoelectronics, Taiyuan University of Technology, Taiyuan, China. Her research interests include nonlinear dynamics of laser diodes and photonic integrated broadband chaotic semiconductor laser.

Zhe Ma received his Ph.D. degree in optical engineering from Tianjin University, Tianjin, China, in 2021. He is currently an associate professor at the College of physics and optoelectronic engineering, Taiyuan University of Technology. His research interests include photoacoustic spectroscopy, fiber optic sensing and photoelectric detection.

Angelo Sampaolo obtained his Ph.D. Degree in Physics in 2017 from University of Bari. He was an associate researcher in the Laser Science Group at Rice University from 2014 to 2016 and associate researcher at Shanxi University since 2018. Since 2023, he is Associate Professor at Polytechnic of Bari. His research activity is focused on the development of innovative techniques in trace gas sensing, based on Quartz-Enhanced Photoacoustic Spectroscopy and covering the full spectral range from near-IR to THz.

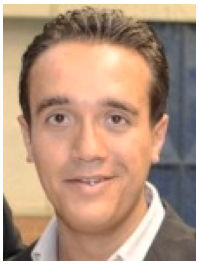

Pietro Patimisco obtained Ph.D. Degree in Physics in 2013 from the University of Bari. Since 2022, he is Associate professor at the Technical University of Bari. He was a visiting scientist in the Laser Science Group at Rice University in 2013 and 2014. Prof. Patimisco's scientific activity addressed the study and applications of trace-gas sensors, such as quartz-enhanced photoacoustic spectroscopy and cavity enhanced absorption spectroscopy in the mid infrared and terahertz spectral region, leading to several publications.

Vincenzo Spagnolo obtained the Ph.D. in physics in 1994 from University of Bari. Since 2004, he works at the Technical University of Bari, formerly as assistant and associate professor and, starting from 2018, as full Professor of Physics. Since 2019, he is vice-rector of the Technical University of Bari, deputy to technology transfer. He is the director of the joint-research lab PolySense between Technical University of Bari and THORLABS GmbH, fellow member of SPIE and senior member of OSA. His research interests include optoacoustic gas sensing and spectroscopic techniques for real-time monitoring.

Hongpeng Wu received his Ph.D. degree in atomic and molecular physics from Shanxi University, China, in 2017. From September, 2015 to October, 2016, he studied as a joint Ph.D. student in the Electrical and Computer Engineering Department and Rice Quantum Institute, Rice University, Houston, USA. Currently he is a professor in the Institute of Laser Spectroscopy of Shanxi University. His research

Lei Dong received his Ph.D. degree in optics from Shanxi University, China, in 2007. From June, 2008 to December, 2011, he worked as a post-doctoral fellow in the Electrical and Computer Engineering Department and Rice Quantum Institute, Rice University, Houston, USA. Currently he is a professor in the Institute of Laser Spectroscopy of Shanxi University. His research interests include optical sensors, trace gas detection, photoacoustic spectroscopy and laser spectroscopy.